TR-236

ATOMIC ENERGY
OF CANADA LIMITED
Research Company

L'ENERGIE ATOMIQUE
DU CANADA, LIMITEE
Société de Recherche

A MAGNETOTELLURIC SURVEY OVER THE EAST BULL LAKE GABBRO-ANORTHOSITE COMPLEX

LEVE MAGNETOTELLURIQUE DU COMPLEXE GABBRO-ANORTHOSITE DE EAST BULL LAKE

R. D. Kurtz, E. R. Niblett

Work directed by
Earth Physics Branch
ENERGY, MINES AND RESOURCES
CANADA
for
ATOMIC ENERGY OF
CANADA LIMITED

Travaux dirigés par
Direction de la physique du globe
ENERGIE, MINES ET RESSOURCES
CANADA
pour
L'ENERGIE ATOMIQUE DU
CANADA, LIMITEE

May 1984 mai

NOTICE

This Technical Record covers ongoing work done as part of the Nuclear Fuel Waste Management Program, and is intended for quick dissemination of the information. The information it contains may not yet have been evaluated rigorously, and any conclusions may be subject to modification in the light of further information.

This report is not to be listed in abstract journals. If it is cited as a reference, the source from which copies may be obtained should be given:

Scientific Document Distribution Office (SDDO),
Atomic Energy of Canada Limited, Research Company,
Chalk River, Ontario K0J 1J0.

Please refer to the TR-number when requesting additional copies of this document. Single copies of this report are available at no charge from SDDO.

Technical Record TR-236

A MAGNETOTELLURIC SURVEY OVER THE EAST BULL LAKE GABBRO-ANORTHOSITE COMPLEX

by

R.D. Kurtz and E.R. Niblett

ABSTRACT

A magnetotelluric survey at the East Bull Lake area (RA 7) in 1982 August included three tensor soundings and 52 scalar observations. The tensor stations were located close to Highway 553, which provided the only available road access to the vicinity of the site. The scalar observations were taken at 100-m intervals along the cut lines 212N, 227N, 265E and 269E. Two new instruments were available for this work: a tensor system produced by Phoenix Geophysics which operates over the frequency range from 0.00055 to 384 Hz; and a scalar system produced by SYGEQ of Montreal covering the range from 1 to 5000 Hz. Near-surface conducting layers were detected at depths ranging from about 50 m near the northeast margin of the gabbro-anorthosite complex to 800 m near the center of the structure. The scalar profiles revealed the presence of prominent low-resistivity zones at depth, most of which correspond to mapped geological faults. The most important of these is the Folson Lake Fault zone transecting the southern portion of the complex.

Division of Seismology and Geomagnetism
Earth Physics Branch
Energy, Mines and Resources Canada

Work done for

Atomic Energy of Canada Limited
Whiteshell Nuclear Research Establishment
Pinawa, Manitoba R0E 1L0
1984 May

Dossier technique TR-236

LEVÉ MAGNÉTOTELLURIQUE DU COMPLEXE GABBRO-ANORTHOSITE DE EAST BULL LAKE

par

R.D. Kurtz et E.R. Niblett

RÉSUMÉ

Un levé magnétotellurique a été effectué dans la région de East Bull Lake (RA 7) en août 1982; il comportait trois sondages tensoriels et 52 visées scalaires. Les postes de sondage tensoriel étaient situés près de l'Autoroute 553 qui était la seule voie d'accès existante pour se rendre à l'endroit étudié. Les visées scalaires ont été faites tous les 100 m le long des lienes de percée 212N, 227N, 265E et 269E. On disposait de deux nouveaux instruments pour ces travaux: un système tensoriel produit par Phoenix Geophysics fonctionnant dans une gamme de fréquences de 0.00055 à 384 Hz et un système scalaire produit par SYGEQ de Montréal fonctionnant dans la gamme de 1 à 5000 Hz. On a détecté des couches conductrices au voisinage de la surface, à des profondeurs s'échelonnant entre environ 50 m prés de la limite nord-est du complexe gabbro-anorthosite et 800 m prés du centre de la structure. Les profils scalaires ont révélé la présence d'importantes zones à faible résistivité à certaines profondeurs; la plupart d'entre elles correspondent aux failles géologiques cartographiées. La plus importante est la zone de la Folson Lake Fault divisant transversalement la partie sud du complexe.

Division de la séismologie et du géomagnétisme
Direction de la physique du globe
Énergie, Mines et Ressources Canada

Travaux effectués pour

L'Énergie Atomique du Canada, Limitée
Établissement de recherches nucléaires de Whiteshell
Pinawa, Manitoba ROE 1LO
1984 mai

CONTENTS

		Page
1.	INTRODUCTION	1
2.	THE MAGNETOTELLURIC METHOD	1
3.	INSTRUMENTATION	3
4.	GEOLOGY	4
5.	GEOPHYSICS	5
6.	MAGNETOTELLURIC SURVEY RESULTS	5
	6.1 TENSOR MT	5
	6.2 ONE-DIMENSIONAL ANALYSIS BY INVERSION	7
	6.3 SCALAR AMT	8
	6.4 AVERAGE SCALAR RESISTIVITY VALUES	10
7.	CONCLUSIONS	10
	ACKNOWLEDGEMENTS	11
	REFERENCES	11
	TABLES	13
	FIGURES	15

1. INTRODUCTION

A magnetotelluric (MT) survey was conducted of the East Bull Lake (RA 7) gabbro-anorthosite complex (Figure 1) during the period 1982 August 9 to 27 by the Earth Physics Branch as part of the Nuclear Fuel Waste Management Program for Atomic Energy of Canada Limited.

The survey was designed to provide depth estimates of the gabbro-anorthosite intrusions, to investigate the electrical character of the Folson Lake Fault zone which transects the southern portion of the structure, and to compare MT results in the region with those acquired by very low frequency (VLF) and other electrical methods. The survey relied on two new MT instruments recently acquired by the Earth Physics Branch: a scalar audio-MT (AMT) system produced by SYGEQ of Montreal, and a tensor system produced by Phoenix Geophysics of Toronto. Tensor soundings were made at three sites where road access was available, and scalar profiling was conducted along cut lines at a total of 52 locations. For the latter work scalar measurements were made in two orthogonal directions at seven frequencies ranging from 8 Hz to 5000 Hz. The tensor data covered the range from 0.00055 Hz to 384 Hz.

2. THE MAGNETOTELLURIC METHOD

The concepts used in the MT technique are described in detail by Vozoff (1972), Strangway et al. (1973) and Kaufman and Keller (1981). A MT sounding is made by measuring naturally occurring electromagnetic signals at the surface of the earth. The magnetic field variations are usually measured by metal-cored induction coils while the simultaneous electric (telluric) field variations are determined by measuring the potential between pairs of electrodes embedded in the earth. The signals are generated by two different source mechanisms, one at audio frequencies and one at subaudio frequencies. In general, signals with periods longer than 1 s result from changes in the earth's magnetic field caused by complex interactions between this field and the flow of plasma from the sun. Measurements with this signal source are usually referred to as magnetotelluric (MT) soundings. The audiomagnetotelluric technique (AMT) normally uses signals with frequencies greater than 1 Hz which are generated by worldwide thunderstorm activity. The energy propagates around the world in a waveguide between the earth's surface and conductive layers in the ionosphere.

A basic scalar sounding involves computing the ratio of one horizontal magnetic component (H) and the orthogonal electric component (E). Since lower-frequency fields penetrate more deeply into the earth, measurements taken at a number of frequencies at one site can provide resistivity information at various depths. The depth of sounding may be related approximately to frequency by the relation

$$\delta \simeq 503.3\sqrt{\rho/f} \qquad (1)$$

where δ = skin depth (m)
ρ = resistivity ($\Omega \cdot m$)
f = frequency (Hz).

The apparent resistivity may be calculated from

$$\rho_a = \frac{1}{5f} \left|\frac{E}{B}\right|^2 \qquad (2)$$

where ρ_a = apparent resistivity ($\Omega \cdot m$)
E = electric field (mV/km)
B = magnetic induction (nT).

If the earth were a homogeneous half space, ρ_a would be the true resistivity. However, in the more realistic case where the earth exhibits changes in resistivity with depth and/or with lateral direction, the MT method actually determines an effective or "apparent" resistivity. This is a complex and frequency-dependent parameter that must be interpreted to estimate the actual distribution of resistivity at various depths.

Scalar soundings, especially scalar AMT soundings, can be carried out quickly and easily with portable equipment. They provide an excellent method for delineating the near-surface structure. In situations where the ground can be considered layered (referred to as the one-dimensional case), the ρ_a values can be interpreted directly by matching field results with theoretical curves or by using an inversion program. In areas of more complex geology, the geoelectric structure can change not only with depth, but also in one horizontal direction (the two-dimensional case) or in all directions (the three-dimensional case). Thus the measurements become direction dependent. In the two-dimensional case, scalar measurements will provide the most useful data when the measuring axes are aligned parallel or perpendicular to the strike of the structure. If this is done, the measured results may be compared with the responses of two-dimensional models and an interpretation can be made.

In general, for non-homogeneous or anisotropic terrains, earth resistivity varies laterally and with depth and the horizontal electric and magnetic field components are related by the linear relation

$$\begin{pmatrix} E_x \\ E_y \end{pmatrix} = \begin{pmatrix} Z_{xx} & Z_{xy} \\ Z_{yx} & Z_{yy} \end{pmatrix} \begin{pmatrix} H_x \\ H_y \end{pmatrix} \qquad (3)$$

The subsripts x and y refer to north and east compenents, respectively, and Z_{xx}, etc. are the elements of the impedance tensor. The apparent resistivity is related to the impedance tensor elements by

$$\rho_{axy} = \frac{1}{5f} \left|Z_{xy}\right|^2 \qquad (4a)$$

and

$$\rho_{ayx} = \frac{1}{5f} \left|Z_{yx}\right|^2. \qquad (4b)$$

Thus, in areas of complex geology or where the strike is unknown, it is useful to make a tensor sounding where the two horizontal magnetic and two electric components are measured simultaneously. Then, if the geoelectric structure has a defined strike direction, the apparent resistivity curves may be computed parallel and perpendicular to the structure by rotating the measurements mathematically. The largest apparent resistivities are found along the major axis of anisotropy while the smallest values (in the two-dimensional case) are at 90° to the major axis. If variations in the vertical magnetic field are also recorded, geomagnetic transfer functions may be computed and these can be used to determine the strike of the structure and its location relative to the recording site.

For a given frequency and a given ensemble of geomagnetic events, the transfer function technique gives a least-squares derivation of the number pair (A,B) that best satisfies the assumed linear relation:

$$Z = AX + BY \tag{5}$$

where X,Y,Z are here regarded as complex Fourier transform estimates of the north, east and vertically downward components of geomagnetic variations. The complex transfer functions (A,B) may be divided into real (in-phase) and imaginary (quadrature) parts (A_R,B_R) and (A_I,B_I). These pairs may, in turn, be expressed as quasi-vectors or arrows with magnitudes

$$M_R = (A_R^2 + B_R^2)^{1/2}, \quad M_I = (A_I^2 + B_I^2)^{1/2} \tag{6a}$$

and azimuths

$$\theta_R = \tan^{-1}(B_R/A_R), \ \theta_I = \tan^{-1}(B_I/A_I). \tag{6b}$$

M_R represents a statistical estimate of the ratio of the correlated parts of in-phase Z to H_R where H_R is the horizontal component that maximizes the correlation and θ_R is its azimuth. Similarly, M_I is an estimate of the ratio of the correlated parts of quadrature Z to H_I and H_I has θ_I as its azimuth. The in-phase induction arrow tends to point towards the strongest conductor in the vicinity of the recording station.

3. INSTRUMENTATION

The SYGEQ scalar AMT system features a built-in microprocessor to handle data acquisition and to directly compute and display the apparent resistivity. Resistivities may be measured at any frequency between 1 Hz and 5000 Hz. The integration time over which the signals are averaged can be set from 1 s to 32 767 s. The telluric dipole length is normally 20 m, but any other convenient length may be used. Fast-response detectors warn the operator when a signal has saturated the input amplifiers even momentarily.

The tensor system produced by Phoenix Geophysics Ltd. is potentially capable of recording and processing data from as many as five MT

stations simultaneously. However, the equipment available for the East Bull Lake survey was sufficient only for single-station operations. The advantages of having more than one station include reduced recording time and significant noise reduction by using the remote reference technique (Gamble et al., 1979). The Phoenix system features real-time data reduction and produces plots of most MT parameters that are continuously updated as data are collected. This information insures that no more time than necessary is spent at any station and can allow on the spot survey design decisions concerning station siting and density. Data may be acquired over six decades of signal from frequencies of 384 Hz to periods of 1820 s. Electric dipoles with length $\leq$ 100 m are typically employed.

Unlike the portable scalar equipment, the tensor system is transported in a three-quarter ton van which can be used to house the computer, the digitizer and the operator while recordings are being made. Once the equipment is installed, data from 384 Hz to 1 Hz can be obtained in under two hours if there is adequate signal. However, recording for as long as 24 hours may be necessary to obtain data at the longest periods.

4. GEOLOGY

The East Bull Lake layered gabbro-anorthosite complex is located approximately 26 km NNW of Massey, Ontario in the Superior Province of the Canadian Shield near the boundary of the Southern Province. A detailed description of the geology of this area is given by Born and James (1978) and by McCrank et al. (1982). The complex has an elliptical plan shape and measures approximately 13 km by 4 km, with the long axis being nearly east-west. Rock composition varies between gabbro and anorthosite and the complex has been recrystallized to the amphibolite facies of mineralization. Some layering in the center of the intrusion suggests that the structure could be a basin (Born and James, 1978). The surrounding rocks are syenite, granites, mafic metavolcanics and diabase. Contacts between these and the gabbro-anorthosite complex appear to be faulted with no evidence of chilled margins or of intrusive relationships. Amphibolite and diabase dykes cut most rock types and are very apparent in the main gabbro body. The most common orientation of the dykes is 300° to 320°. The geology of the test area is illustrated in Figure 1.

A number of faults have been mapped in the area, the most important of which is the Folson Lake Fault zone, crossing the southern half of the complex in an ESE-WNW direction. Crystalline rocks affected by this fault, such as those in the gabbro-anorthosite complex, exhibit cataclastic textures, including randomly oriented fractures, angular breccia fragments and numerous microfaults.

5. GEOPHYSICS

The results of only a few preliminary geophysical studies across the East Bull Lake complex are currently available. A gravity survey of 164 observations (Watson, 1982) indicates a mass excess that is related to the mapped outline of the complex. The Bouguer anomaly map is characterized by a strong NE gradient of approximately 22 $\mu m/s^2$ per km. Inversion modeling indicates that the maximum depth of the gabbro could range from 500 to 770 m.

A combined airborne electromagnetic magnetic/VLF-EM survey of 660 line kilometers was flown during 1981 November-December (Paterson and Reeves, 1982). The main features revealed by the VLF-EM data are broad anomalies trending WNW. One prominent anomaly clearly coincides with the Folson Lake Fault zone. Most of the electromagnetic anomalies are coincidant with VLF-EM anomalies and are associated with faults and/or conductive overburden. The overburden is seen to be generally thin (less than 10 m) with moderate resistivity of the order of 100 to 500 $\Omega \cdot m$.

The preliminary report of Soonawala et al. (1982) included two reversed hammer seismic profiles, one approximately 3 km north of East Bull Lake and the second immediatey to the south of the lake. Both indicated the overburden thickness to be less than 10 m. The results of a ground VLF survey west of Half Moon Lake indentified a number of conductors observed on the airborne survey. These VLF conductors will be discussed Section 6.3.

6. MAGNETOTELLURIC SURVEY RESULTS

6.1 TENSOR MT

The Phoenix system was used to measure tensor MT parameters at three locations east and south of East Bull Lake (see Figure 2). Stations could not be established in the central gabbro zone west of Half Moon Lake and on the Folson Lake Fault zone because of limited road access and a lack of cleared areas adjacent to Highway 553.

Transfer function estimates were possible at all three stations (EBL1, EBL2, EBL3) over the frequency range from 1 Hz to 100 Hz. In all cases the in-phase arrows tended to point south, indicating the presence of a conducting zone or current channel in that direction. The amplitudes of the arrows were small (less than 0.2) at each station and did not display any systematic change between stations. Therefore, at these frequences the magnetic field did not appear to be responding to any single local structure such as the Folson Lake Fault zone. Figure 2 illustrates the amplitudes and azimuths of the in-phase arrows at 10 Hz, where the transfer functions were well determined.

Figure 2 also shows the polarization azimuth of the horizontal telluric field from 0.001 Hz to 384 Hz for each station. This direction normally coincides with the azimuth of the major axis of anisotropy of the impedance tensor. The existence of a defined magnetic transfer function and

polarization direction for the telluric fields indicates a lateral change in conductivity is influencing the MT results since a simple layered structure produces no transfer function and has no preferred direction for the telluric field. The apparent resistivity curves in Figures 3, 4 and 5, which are plotted in the major and minor axes of anisotropy, also indicate a multi-dimensional situation. In these figures a large separation is evident in the amplitude of the apparent resistivity curves that are measured with telluric fields parallel and perpendicular to the strike of the structure.

To illustrate the behavior of the MT parameters in the vicinity of a lateral change in conductivity, consider a simple two-dimensional structure that consists of a vertical fault separating material having different resistivities on either side. At a location on the more resistive side, the apparent resistivity measured parallel to the fault will be lower than that measured perpendicular to it (Vozoff, 1972). At high frequencies (where the skin depth is small relative to the distance to the fault), the two curves will asymptotically approach the resistivity value of the resistive side. At locations on the more conductive side, the apparent resistivity measured parallel to the fault will be higher than that measured perpendicular to it. Again, at high frequencies the two surves will asymptotically approach the resistivity value for the more conductive side. The transfer function has maximum amplitude near the fault and decreases smoothly to zero on both sides.

In two- or three-dimensional situations, there should be a density of stations sufficient to locate the boundaries of all structures so that the data can be modeled with a computer program that accounts for all conductivity changes. Unfortunately such programs are expensive to use and are not readily available; programs that can model two-dimensional structures are in common use. The skew of the impedance tensor (Vozoff, 1972), i.e., the quantity

$$\frac{Z_{xx} + Z_{yy}}{Z_{xy} - Z_{yx}}$$

is useful to compute because it provides a measure of the dimensionality or complexity of the structure in the vicinity of the recording site. The skews computed at EBL1 and EBL3 were small, indicating that these stations are located near structures which are predominantly two-dimensional. At EBL2 the skew was larger (0.2 to 0.35), which indicates a slightly more complex environment.

A two-dimensional interpretation would be valid for these three stations, but without sufficient stations to delineate conductivity contrasts in the vicinity of the observing sites, it would be premature to attempt such model studies. However, two-dimensional model studies indicate that the true apparent resistivity curve (that which would be measured if lateral contrasts were absent) often lies between the curves corresponding to the major and minor axes of anisotropy, especially in cases where the two curves do not cross and remain essentially parallel to long periods (see Figures 3, 4 and 5). In these cases the curve for the telluric field

measured parallel to the strike of the contrast is usually closer to the true curve.

The telluric field at EBL1 was strongly polarized at an angle of about 66° west of north. This information, when combined with the transfer function direction, could indicate that the station is situated in an area that is more conductive than the region to the northeast. Therefore, the major apparent resistivity curve at EBL1 could be considered more representative of the electrical structure beneath the station. The telluric field polarizations and the transfer functions at EBL2 and EBL3 indicate that each could be on the resistive side of a conductivity contrast located to the south (though not necessarily the same contrast). The minor apparent resistivity curves could be the most representative of structure beneath these two stations.

6.2 ONE-DIMENSIONAL ANALYSIS BY INVERSION

Apparent resistivity and phase data for the three tensor stations in the major and minor axes of anisotropy are given in Figures 3, 4 and 5. The data for EBL1 and EBL3 were derived by merging two recordings made at each station. With a few exceptions, only data with multiple coherencies (Reddy and Rankin, 1974) greater than 0.8 were used at EBL1 and EBL2. It was necessary to use a lower criterion at EBL3 because of very low signal levels and wind-related noise (see Table 1).

As discussed in the previous section, only a one-dimensional interpretation of the data is justified at the present time. Therefore, the data were inverted to a conductivity-depth profile by using the programs of Oldenburg (1979). The inversion procedure is an objective process that uses the apparent resistivity and phase data to produce a model that provides a reasonable match of the model responses to the observations.

The inversion process is performed in two stages. The first stage computes a conductivity function continuous with depth from a given starting model by an iterative procedure that attempts to reproduce the data to within an accuracy determined by their statistical errors. The data used in the inversion process are indicated by solid symbols in Figures 3 and 4. The response of the inversion model is shown by the solid curves in these figures. The second stage appraises the features of the model to determine their significance. Oldenburg discusses a spread criterion, S, which is an indication of the resolution of structure at depth. The profiles of conductivity vs. depth and the spread resulting from the inversion are given in Figures 6 to 9. On the depth range where the spread function lies to the left of the diagonal line (part "b" of each figure), the resistivity vs. depth curve is well resolved. The spread function plots clearly illustrate that conductive layers tend to be well resolved with the MT method, while resistive zones lying between conductive layers are only poorly resolved.

In Figure 6 there is evidence for a conductive feature at a depth of between 50 to 100 m at EBL1. There are also conductors near 2 km and 25 km. The lower two conductors may be similar to crustal features in the Grenville Province north of Québec City discussed by Kurtz (1982). The long-period data defining these conductors will be studied in greater detail once additional soundings are obtained.

Based on reasoning in the last section, the data in the major axis of anisotropy are likely more representative of structure beneath EBL1. Since it is not possible to be definite about this choice, the minor curve data were also inverted. The inversion results in Figure 7 for the minor curves at EBL1 also show conductors below 60 m and below 2 km. Even though the major and minor curves display a relatively large anisotropy, both indicate a significant conductor at depths below 50 to 100 m. Two-dimensional models are required before more can be said about its conductivity and thickness.

As previously discussed, the minor apparent resistivity and phase curves at EBL2 were chosen as most representative of structure below the station. Here, the near-surface conductor begins to appear below the depth of 100 m. Also there is a second well-resolved conductor below 3 km (Figure 8).

For completeness, the data for the major apparent resistivity and phase at EBL2 were inverted, with the results shown in Figure 9. These results indicate a conductor at depths below 300 m, but the spread indicates it is not very well resolved.

The data from EBL3 (Figure 5) are of poor quality because of wind-generated noise and low signal levels. Nonetheless, the curves show the trend to lower resistivities for frequencies higher than 30 Hz. This indicates a shallow conductor exists below this station as well.

6.3 SCALAR AMT

Scalar AMT soundings were made along cut lines 212N, 227N, 265E and 269E as indicated by the solid squares in Figure 2. Soundings were taken with the telluric lines orientated north-south and then east-west. Resistivity values were recorded at even frequencies which ranged from 8 Hz to 5000 Hz. Figures 10 to 13 show the data plotted in the form of pseudo-sections for both orientations of the telluric dipole. These are plots of the resistivity as a function of frequency along the four profile lines. The highest frequencies are on the top and the lowest on the bottom to give an idication of the change in resistivity with depth. The resistivity values are contoured to more clearly reveal the structure.

6.3.1 Line 212N (Figure 10)

Stations were occupied at 100-m intervals from the first steel marker (282E) west of Highway 553 to line 265E. The resistivity appears to be lower in the vicinity of 250 Hz, especially for the north-south orientation of the telluric dipole. Four conductive zones are readily observed.

6.3.1.1 265E - 267E

This is a complex geological zone (McCrank, 1982) that includes a fault striking WNW (Born and James, 1978). In addition, the surface is swampy which may account for the low resistivity at 5000 Hz. An airborne VLF-EM anomaly is observed between stations 265E and 266E (Paterson and Reeves, 1982).

6.3.1.2 269E

This conductive feature is evident only for the E-W telluric field orientation. There is nothing to indicate its origin on the geological maps. It coincides with a minor topographic low.

6.3.1.3 274E

Stations in the vicinity of 274E are in or near the Folson Lake Fault zone. This area is low and swampy, which may account for the low resistivity observed at 5000 Hz for both orientations of the telluric dipole. There is also a strong airborne VLF-EM anomaly associated with this feature. A pronounced conductivity low at 250 Hz extends to station 270E.

6.3.1.4 280E - 282E

There is evidence for a conductor at some depth in the granodiorite.

6.3.2 Line 265E (Figure 11)

This line cuts north-south through the central gabbro intrusion. There is evidence for a low-resistivity zone over much of this profile centered at 250 Hz for both orientations of the telluric dipole. In addition, attention is drawn to the following resistivity lows.

6.3.2.1 212N - 213N

This appears to be the northward extension of the anomaly observed on L212N, stations 265E to 267E. There are three faults identified by Born and James (1978) in this area. Also there is a continuation of the airborne VLF-EM anomaly WNW across this profile.

6.3.2.2 215N - 217N

The Folson Lake Fault zone coincides with the high conductivity centred at 250 Hz in this section of the profile. Again there is a strong airborne VLF-EM anomaly (Paterson and Reeves, 1982) and a ground VLF-EM anomaly (Soonawala et al., 1982).

6.3.2.3 224N

The conductor centered at 224N coincides with a ground VLF-EM anomaly (Soonawala et al., 1982) and appears to continue to L269E (Figure 12). The low resistivity at 5000 Hz is probably caused by the shallow conductor seen by the VLF survey. There is no significant topographic feature associated with this anomaly.

6.3.3 Line 269E (Figure 12)

The AMT signature along this line is fairly uniform, especially for the telluric E-W orientation. The lowest apparent resistivity values collected in the survey occur at 222N, which is 75 m north of the ground

VLF-EM anomaly (Soonawala et al., 1982) and in a topographic low. The pseudosection at this anomaly is very similar to that at 224N on L265, especially for the telluric electrodes N-S.

The resistivity low observed near the surface at 225N coincides with a ground VLF-EM anomaly reported by Soonawala et al. (1982). A deeper conductor centred at 250 Hz is evident for both field orientations.

6.3.4 L227N (Figure 13)

Both orientations show a distinctive low resistivity zone starting at 272E and continuing westward to 265E and perhaps beyond. The anomaly at 270E could be related to a fault mapped by Born and James (1978). An airborne VLF-EM anomaly striking NW is also observed at this location (Paterson and Reeves, 1982).

6.4 AVERAGE SCALAR RESISTIVITY VALUES

Scalar apparent resistivity values can be dominated by near-surface effects on the electric field. Therefore, it is difficult to choose any one site that might be representative of the structure at depth. Six scalar sites were chosen that displayed small anisotropy in the orthogonal measuring directions and were isolated from the lateral conductive anomalies identified in the pseudosections. These stations were in the central core of the intrusion north of the Folson Lake Fault zone. The stations and apparent resistivity values are shown in Table 2. The mean and standard deviation (SD) were computed for

$$X = \frac{1}{N} \sum_{i=1}^{N} \log_{10} (\rho_a i) \qquad (7)$$

Then

$$\rho \text{ average} = 10^{X}$$
$$\rho \text{ maximum} = 10^{X+SD}$$
$$\rho \text{ minimum} = 10^{X-SD}.$$

The averaged results are plotted in Figure 14 for the telluric N-S and E-W measurements. Note that the averaged results are nearly isotropic. Since the six stations displayed small anisotropy it was assumed structure in their vicinity was nearly one-dimensional. Therefore the one-dimensional inversion technique was applied to the telluric N-S data with the results shown in Figure 15. A conductive zone is resolved below 800 m.

7. CONCLUSIONS

The scalar profiling results represented by the pseudosections of Figures 10 to 13 give a strong impression of the gross structural character of the gabbro region between the surface and depths of a few kilometers. We see evidence of a complex and heterogeneous region. The scalar data clearly identified all faults mapped by Born and James (1978) that crossed the profiles. In addition, all VLF-EM anomalies detected by Paterson and Reeves

(1982) and Soonawala et al. (1982) were observed on the scalar AMT data. The significant new feature found at L212N, 279E-282E requires further study. No attempt has been made to model any of the conductive structures to determine their dip. A more detailed scalar survey is required with the telluric dipole oriented perpendicular and parallel to the strike of these important conductive structures before attempts can be made at such modeling. However, an attempt was made to provide a layered-model interpretation of selected scalar AMT data. The preliminary analysis indicates a conductive zone at some depth below 800 m near the center of the gabbro-anorthosite complex. A tensor sounding near the middle of L265 and/or L269 would test the validity of this result.

It is very important to recognize that the one-dimensional layered interpretation is a gross simplification of the geological structure of the gabbro-anorthosite complex. The AMT pseudosections, the VLF studies and the geological reports all indicate the existence of significant lateral contrasts in conductivity throughout this region. Therefore, the inversion results must be viewed with caution since lateral contrasts can result in distortions to the apparent resistivity curves and hence modify the depth to and even the existence of the conducting layers. Once the extent and strike direction of the lateral contrasts are identified, more realistic two-dimensional models can be derived which should provide a more reliable basis for interpreting the structure. With these reservations in mind, the one-dimensional layered inversion results suggest near-surface conducting layers below or near station EBL1 commencing at a depth of 50 to 100 m, at station EBL2 at a depth of 100 to 300 m and below the central gabbro zone west of Half Moon Lake at a depth of about 800 m. If this low-resistivity material underlies the bottom of the gabbro-anorthosite complex, then the complex must thicken substantially from its northeast edge near EBL1 towards its center. The low resistivity could be caused by a fluid-saturated fractured and sheared zone at the base of the complex or perhaps by a lithological change in the rock. However, it should be noted that there may be no structural link between the near-surface conductor observed at EBL1 and EBL2 and the one observed at 800 m near the center of the complex. Additional tensor and scalar MT surveys are required to confirm this hypothesis and to further extend the structural interpretation.

ACKNOWLEDGEMENTS

We are grateful to Jean Legault, Marc Lambert and Dan Krentz for their assistance with the data collection. The reviews of this report by A.G. Green and P.A. Camfield are greatly appreciated.

REFERENCES

Born, P. and R.S. James. 1978. Geology of the East Bull Lake layered gabbro anorthosite intrusion, district of Algoma, Ontario. In: "Current Research, Part A," pp. 91-95, Geological Survey of Canada Paper 78-1A, Supply and Services Canada, Ottawa.

Gamble, T.D., W.M. Goubau and J. Clark. 1979. Magnetotellurics with remote magnetic reference. Geophysics 44, 53-68.

Kaufman, A.A. and G.V. Keller. 1981. The magnetotelluric sounding method. Elsevier Scientific Publishing Company, New York.

Kurtz, R.D. 1982. Magnetotelluric interpretation of crustal and mantle structure in the Grenville Province. Geophys. J. R. Astron. Soc. 70, 373-397.

McCrank, G.F.D., D. Stone, D.C. Kamineni, B. Zayachkivsky and G. Vincent. 1982. Regional geology of the East Bull Lake area, Geological Survey of Canada, Open File Report 873. Unpublished report available from Geological Survey of Canada, 601 Booth Street, Ottawa, Ontario K1A 0E8.

Oldenburg, D.W. 1979. One-dimensional inversion of natural source magnetotelluric observations. Geophysics 44, 1218-1244.

Paterson, N.R. and C.V. Reeves. 1982. Helicopter-borne geophysial surveys of East Bull Lake area, Research Area RA 7, Algoma District, Ontario. Unpublished report by Paterson, Grant and Watson Ltd., GPH-82-159, available from Applied Geoscience Branch, Whiteshell Nuclear Research Establishment, Pinawa, Manitoba R0E 1L0.

Reddy, I.K. and D. Rankin. 1974. Coherence functions for magnetotelluric analysis. Geophysics 39, 312-320.

Soonawala, N., A. Samchek and B. Kerby. 1982. Preliminary report of ground geophysics at East Bull Lake. Unpublished report, GPH-82-140, available from Applied Geoscience Branch, Whiteshell Nuclear Research Establishment, Pinawa, Manitoba R0E 1L0.

Strangway, D.W., C.M. Swift and R.C. Holmer. 1973. The application of audio-frequency magnetotellurics (AMT) to mineral exploration. Geophysics 38, 1159-1175.

Vozoff, K. 1972. The magnetotelluric method in the exploration of sedimentary basin. Geophysics 37, 98-141.

Watson, R.K. 1982. A gravity survey of East Bull Lake intrusion, Research Area RA 7, Algoma District, Ontario. Unpublished report by Paterson, Grant and Watson Ltd., GPH-82-124, available from Applied Geoscience Branch, Whiteshell Nuclear Research Establishment, Pinawa, Manitoba R0E 1L0.

TABLE 1

MULTIPLE COHERENCIES

	FRQ/PRD	EBL1				EBL2		EBL3			
		RECORDING #1		#2		#1		#1		#2	
		MINOR	MAJOR	MINOR	MAJOR	MAJOR	MINOR	MAJOR	MINOR	MAJOR	MINOR
1	384.0000 Hz				0.849		0.850			0.659	
2	288.0000 Hz				0.937		0.887			0.613	
3	192.0000 Hz	0.882	0.883	0.961	0.935	0.579	0.741			0.573	
4	144.0000 Hz	0.957	0.982	0.922	0.953	0.871	0.944	0.751	0.919	0.742	0.904
5	96.0000 Hz	0.951	0.965			0.887	0.971	0.765	0.929	0.681	0.928
6	72.0000 Hz	0.946	0.921			0.892	0.912	0.753	0.893	0.656	0.875
7	48.0000 Hz	0.951	0.978			0.921	0.961			0.641	
8	36.0000 Hz	0.960	0.980			0.930	0.968		0.898	0.635	
9	24.0000 Hz	0.965	0.981			0.901	0.953		0.900	0.681	
10	18.0000 Hz	0.951	0.974			0.907	0.950		0.799	0.676	0.892
11	12.0000 Hz	0.957	0.966			0.880	0.942		0.819		0.791
12	9.0000 Hz	0.961	0.974			0.873	0.943	0.609	0.918		
13	6.0000 Hz	0.922	0.940			0.714	0.770				
14	4.5000 Hz	0.894	0.904			0.726	0.839				
15	3.0000 Hz	0.900	0.900	0.897	0.905	0.762	0.796				
16	2.2500 Hz	0.916	0.903	0.873	0.889	0.771	0.800				
17	1.5000 Hz	0.811	0.757								
18	1.1250 Hz		0.691					0.879			
19	1.3333 s	0.820	0.764	0.926	0.907			0.935	0.953		
20	1.7778 s			0.953	0.937						
21	2.6667 s			0.979	0.975	0.864	0.837				
22	3.5556 s			0.984	0.980	0.923	0.910				
23	5.3333 s			0.989	0.986	0.917	0.879	0.801			
24	7.1111 s			0.989	0.987	0.945	0.937	0.866			
25	10.6667 s			0.991	0.990	0.972	0.971				
26	14.2222 s		0.927	0.985	0.983	0.980	0.977				
27	21.3333 s		0.992	0.982	0.980	0.966	0.971	0.868			
28	28.4444 s		0.981	0.974	0.972	0.980	0.978	0.925	0.863	0.819	
29	42.6667 s			0.985	0.987	0.983	0.983	0.885	0.773	0.917	
30	56.8889 s			0.979	0.979	0.979	0.979	0.907	0.799	0.866	
31	85.3333 s			0.977	0.971	0.984	0.980	0.960	0.809	0.910	
32	113.7778 s			0.978	0.975	0.977	0.974	0.974	0.849	0.951	
33	170.6667 s			0.969	0.951	0.945	0.956	0.914	0.804	0.969	
34	227.5556 s			0.963	0.953	0.957	0.976	0.911	0.817	0.905	
35	341.3333 s			0.963	0.950	0.979	0.982	0.905			
36	455.1111 s				0.933	0.955	0.965	0.812			
37	682.6667 s				0.733	0.981	0.977				
38	910.2222 s			0.969	0.852	0.953	0.964				
39	1365.3333 s										
40	1820.4444 s			0.960	0.575						

TABLE 2

APPARENT RESISTIVITIES

TELLURICS NORTH-SOUTH (kΩ•m)									
Hz	L265 218	L265 219	L265 221	L227 268	L269 219	L269 220	a Average	a Maximum	a Minimum
8	19.9	6.80	10.5	14.6	18.8	17.9	13.8	20.3	9.4
26	10.2	8.53	8.79	10.1	12.4	11.6	10.2	11.6	8.9
70	9.68	9.51	9.75	2.1	3.88	11.9	6.7	12.5	3.5
250	4.33	4.97	4.37	4.3	4.64	7.78	4.9	6.1	4.0
700	7.68	8.92	11.0	12.4	7.41	6.30	8.7	11.0	6.9
1500	23.2	12.8	20.7	14.4	8.36	11.1	14.2	20.2	10.0
5000	15.8	6.98	20.3	8.5	4.87	11.6	10.1	16.4	6.2

Hz	L265 218	L265 219	L265 221	L227 268	L269 219	L269 220	a Average	a Maximum	a Minimum
8	21.2	16.7	17.9	21.4	15.2	13.5	17.4	20.6	14.7
26	9.58	9.76	8.68	10.8	9.05	8.96	9.4	10.1	8.8
70	4.90	6.99	5.97	4.2	4.06	7.30	5.4	6.8	4.3
250	5.53	5.78	3.64	4.5	3.73	6.02	4.8	5.9	3.9
700	12.8	7.96	5.62	14.4	4.02	7.07	7.9	12.2	5.0
1500	39.2	10.6	8.66	17.6	7.18	10.8	13.0	22,9	7.4
5000	24.9	6.50	25.0	3.8	6.31	5.83	9.1	18.9	4.4

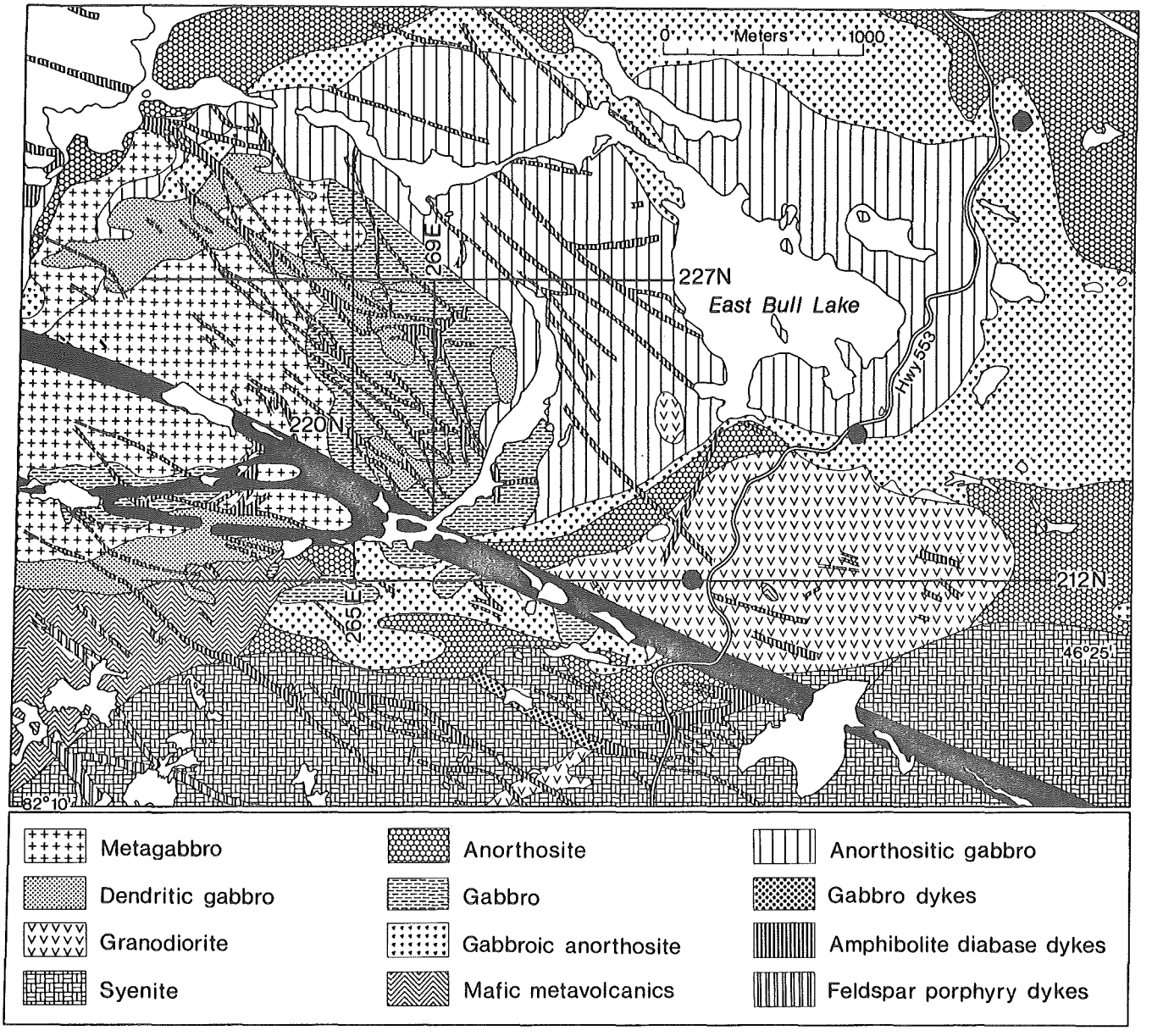

FIGURE 1: Geology of the East Bull Lake Area (from McCrank et al., 1982) [The WNW trending black band represents the Folson Lake Fault Zone. The large dots show the location of the tensor sounding stations.]

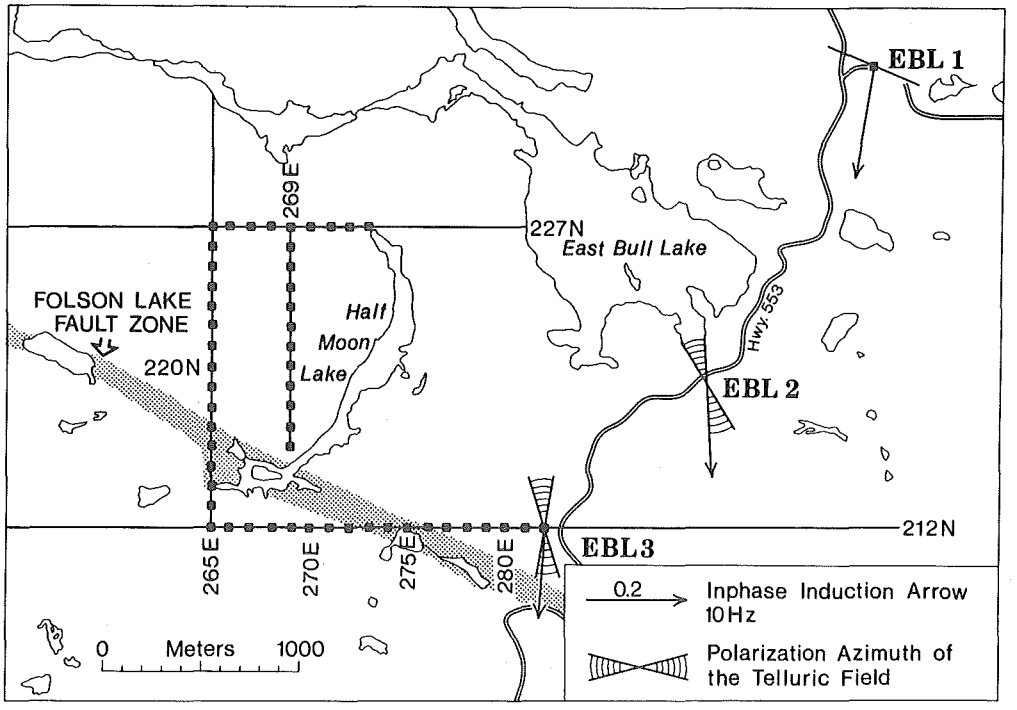

FIGURE 2: Location Map of the Scalar and Tensor Magnetotelluric Stations

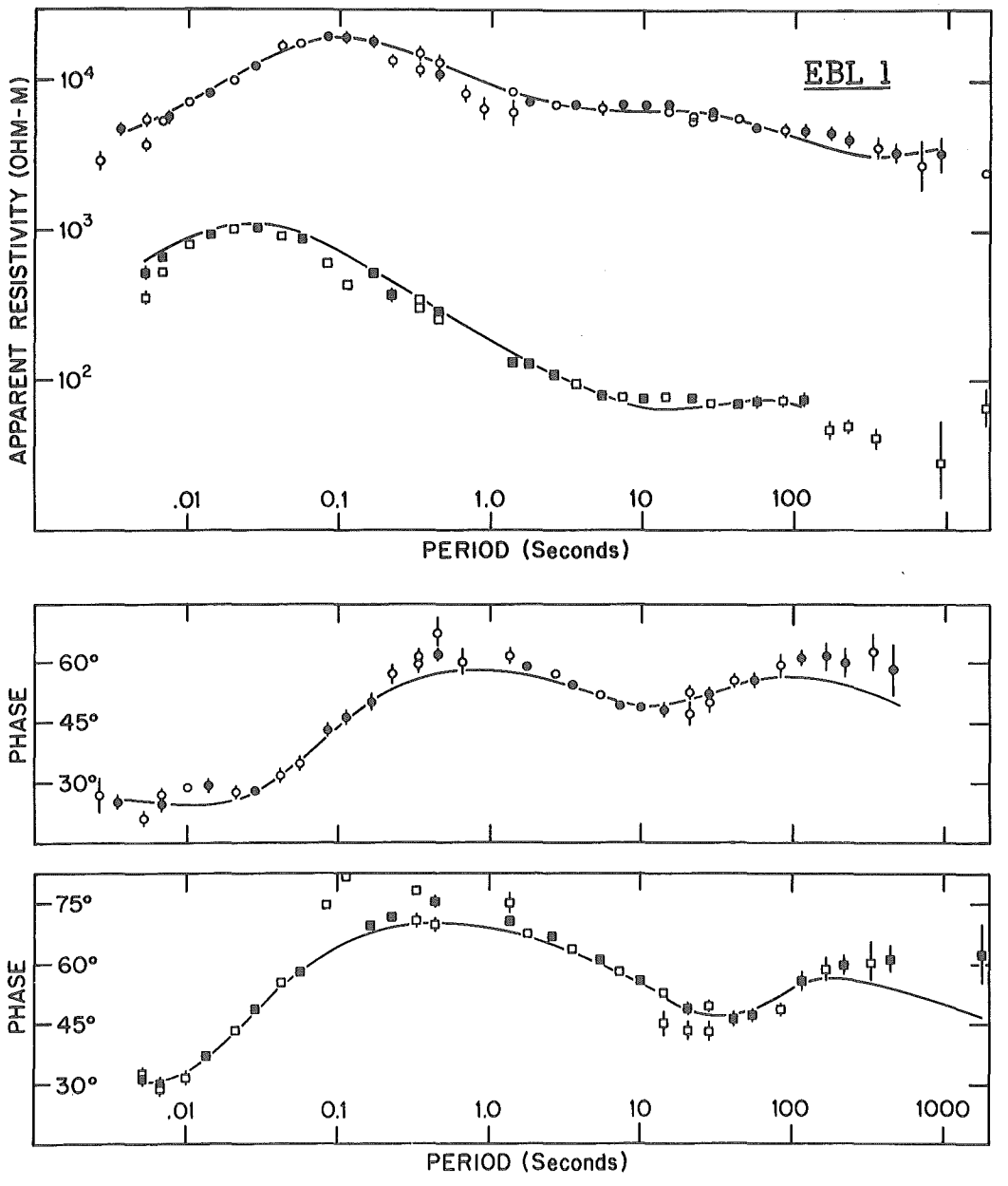

FIGURE 3: Tensor Apparent Resistivity and Phase Results in the Major and Minor Axes of Anisotropy at EBL1 [Solid symbols represent data used in the inversion process. Solid lines are the response of the conductivity versus depth model produced by the inversion program.]

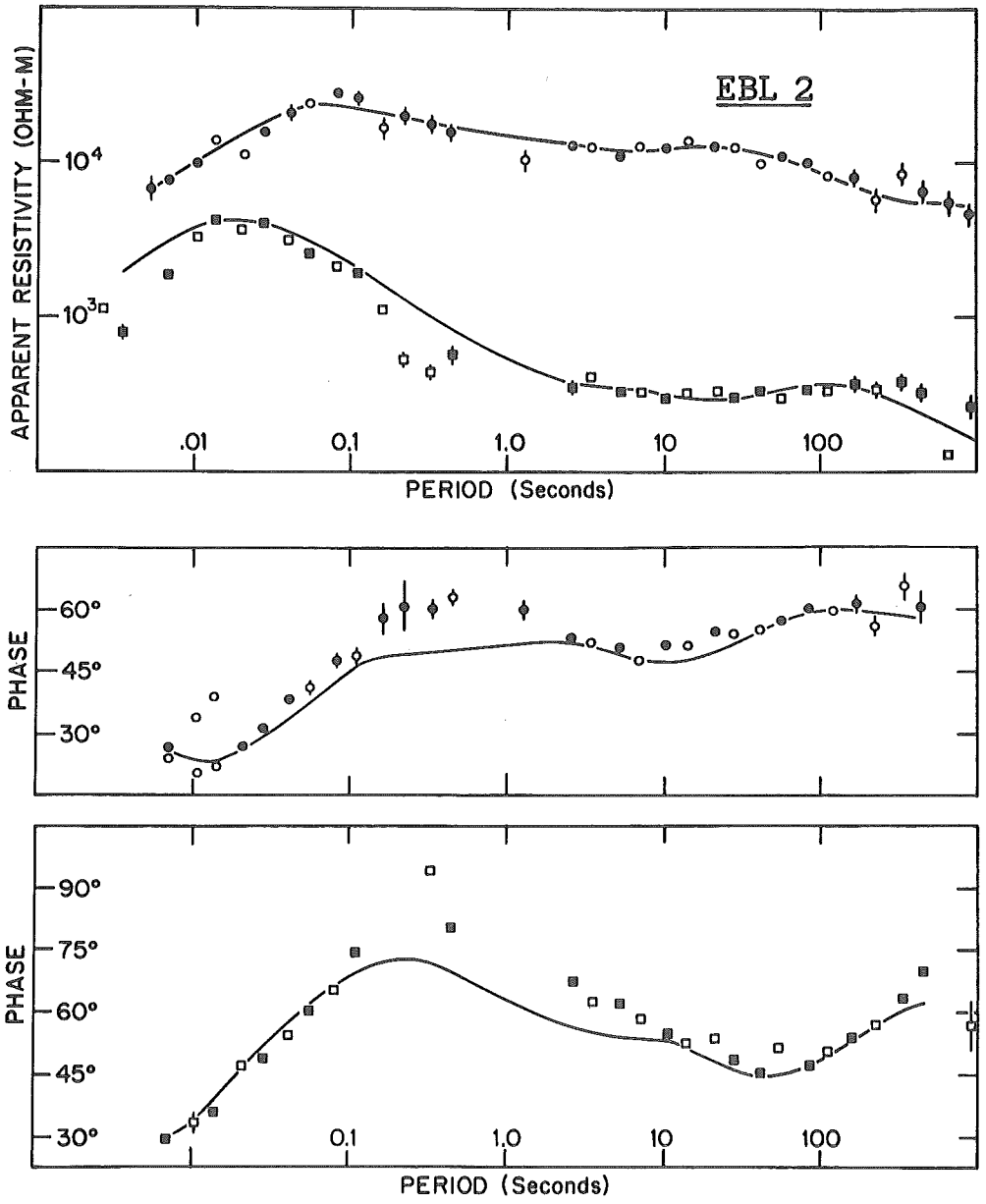

FIGURE 4: Tensor Apparent Resistivity and Phase Results in the Major and Minor Axes of Anisotropy at EBL2 [Solid symbols represent data used in the inversion process. Solid lines are the response of the conductivity versus depth model produced by the inversion program.]

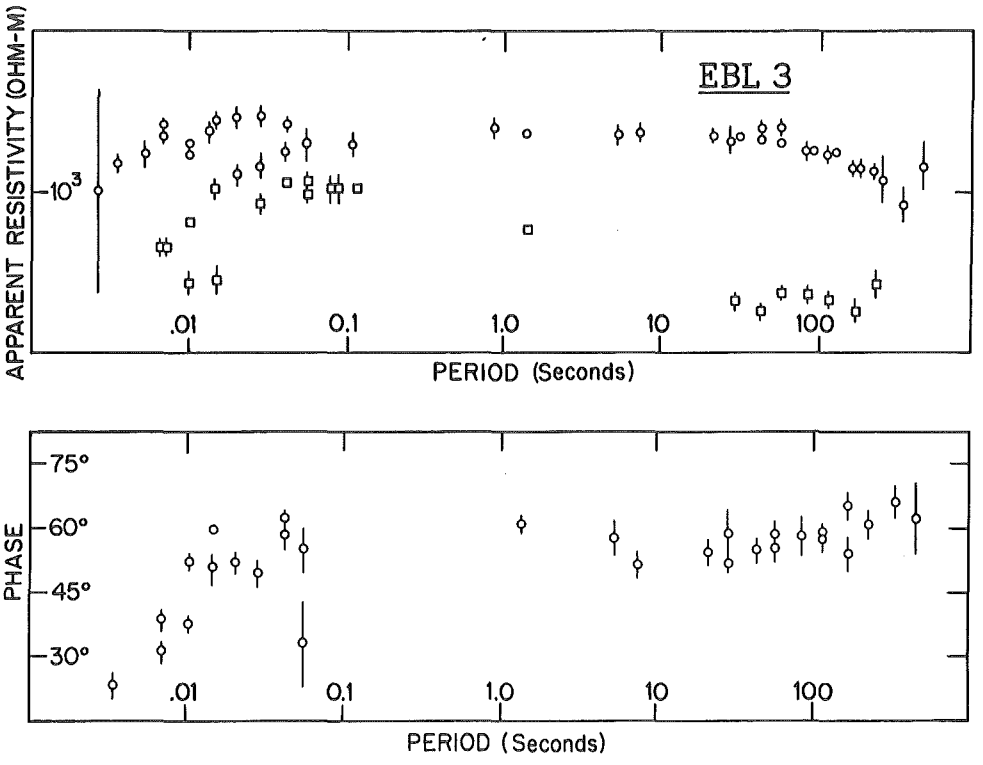

FIGURE 5: Tensor Apparent Resistivity for EBL3 in the Major and Minor Anisotropy [Phase in the minor axis was not well determined and is not displayed]

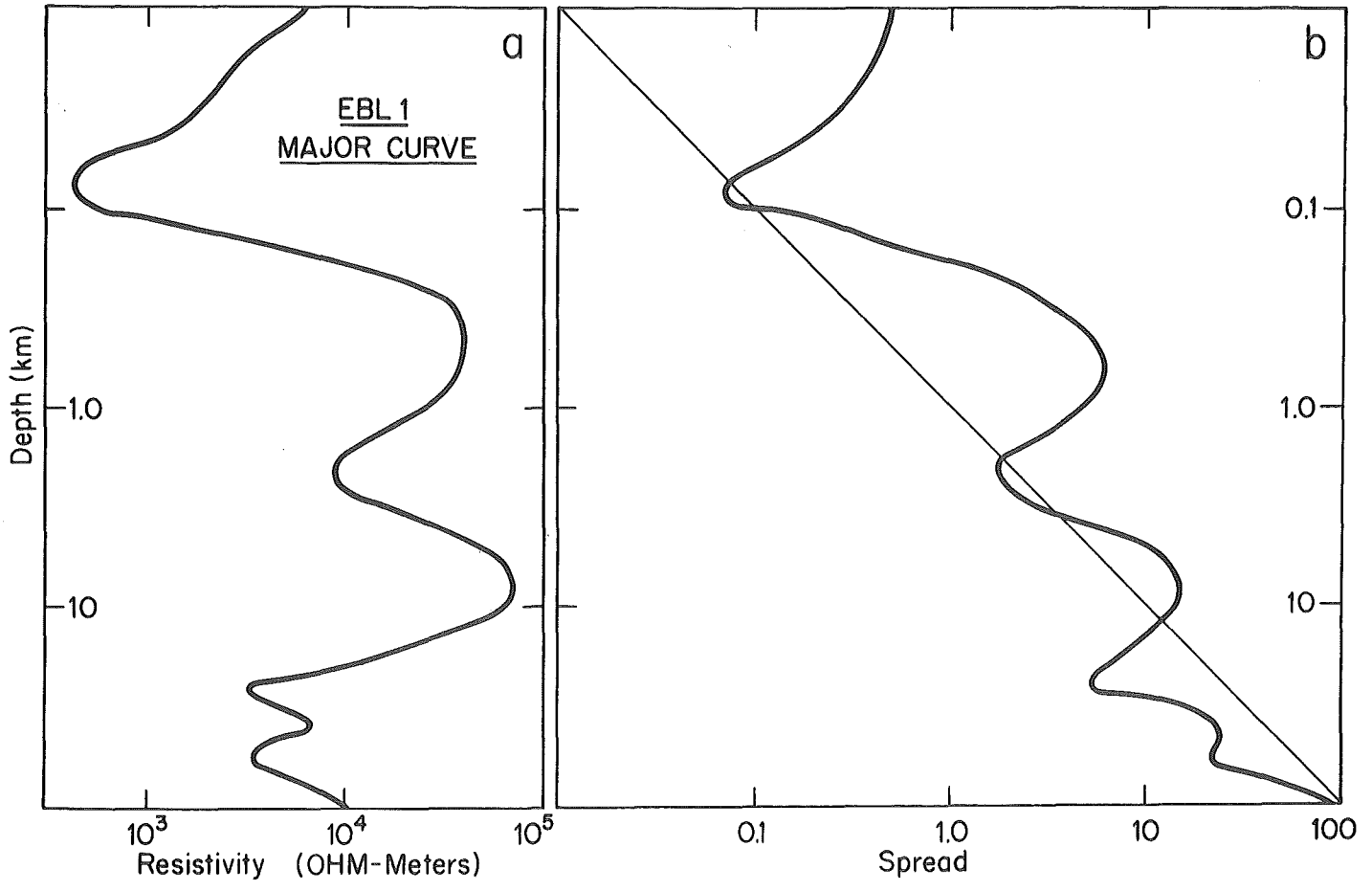

FIGURE 6: (a) Resistivity versus Depth Model Generated by the Inversion Process for Data from EBL1, Major Axis
(b) The Spread Function for the Resistivity Model [Spread values to the left of the 45° line indicate depths at which the conductivity is well resolved.]

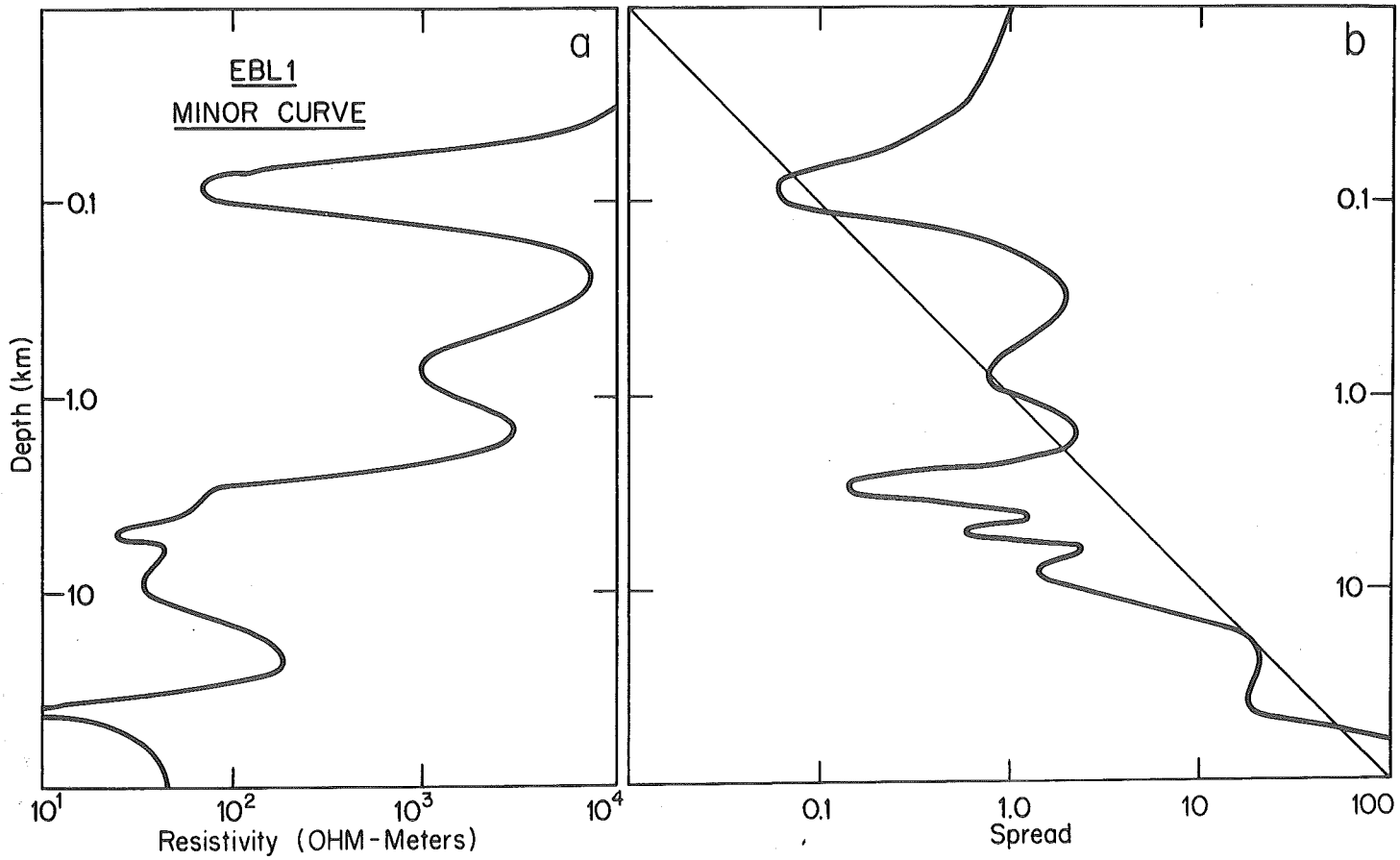

FIGURE 7: Same as Figure 6 for Data from EBL1, Minor Curve

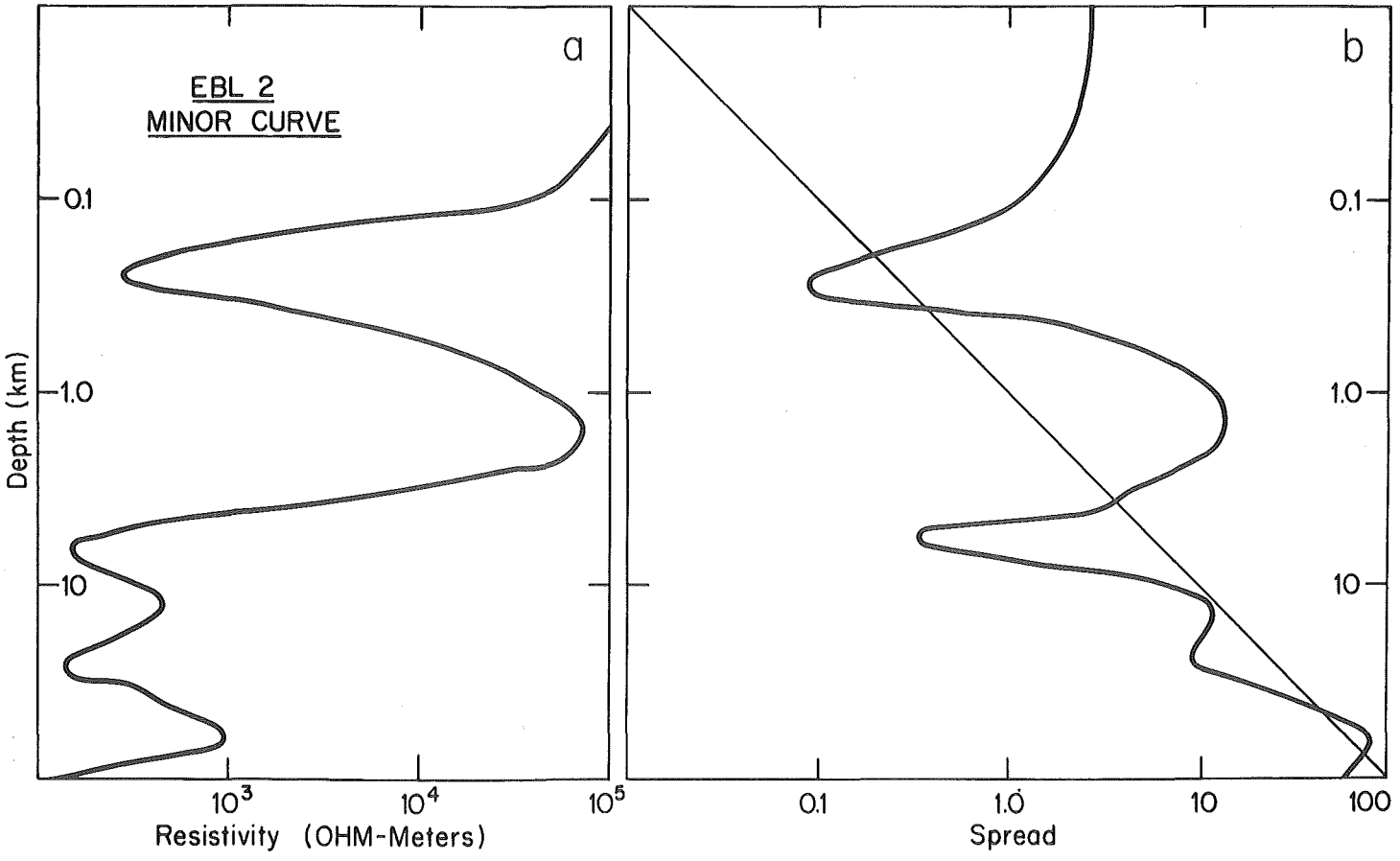

FIGURE 8: Same as Figure 6 for Data from EBL2, Minor Curve

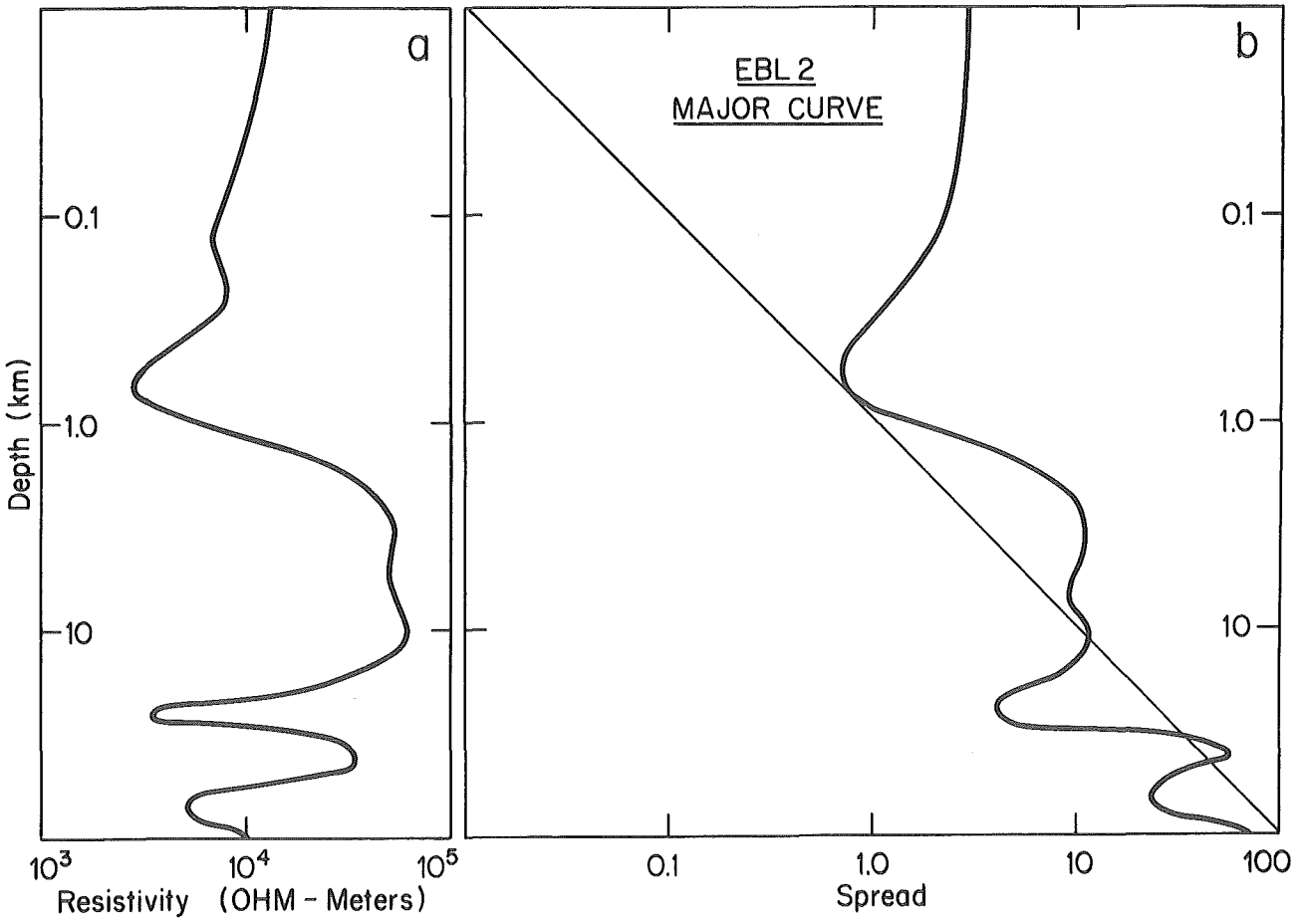

FIGURE 9: Same as Figure 6 for Data from EBL2, Major Curve

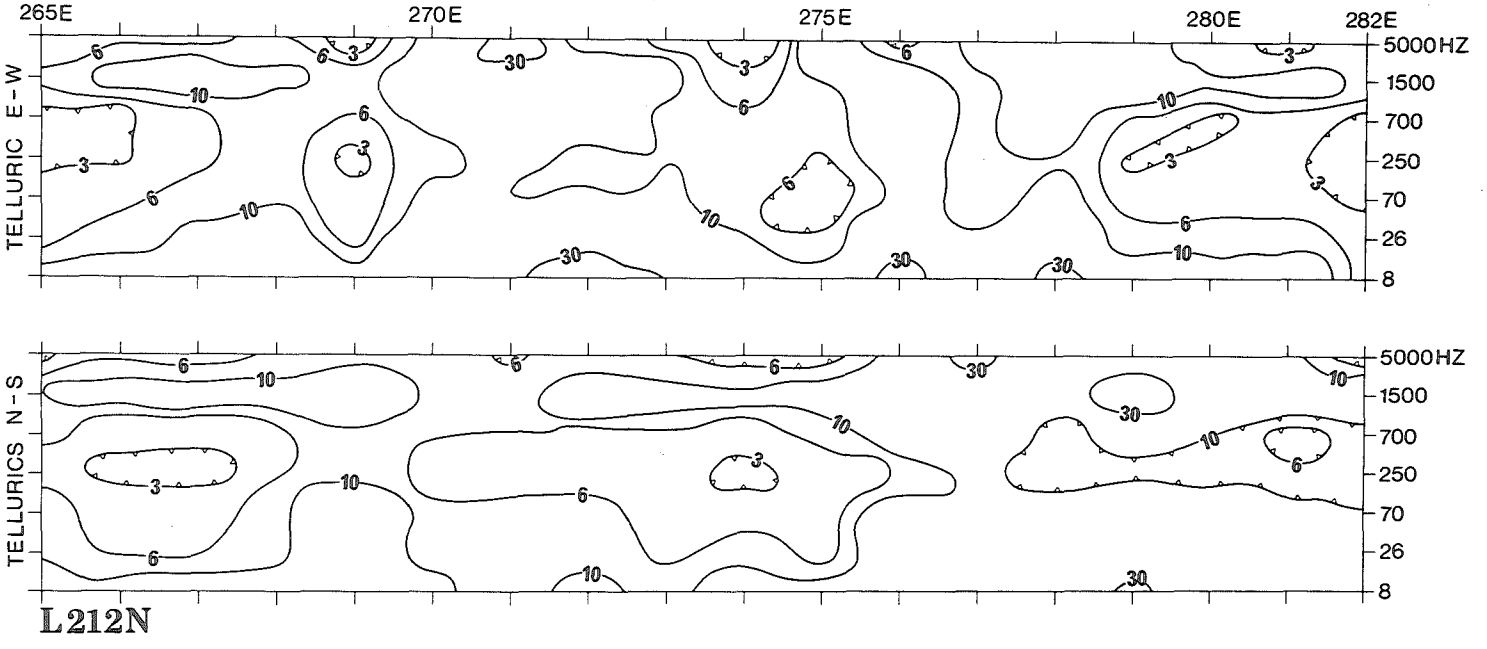

FIGURE 10: Pseudosections for the Scalar AMT Data Measured with the Telluric Dipole East-West (upper section) and with the Telluric Dipole North-South (lower section) for Line 212N [Contours are measured in kΩ•m]

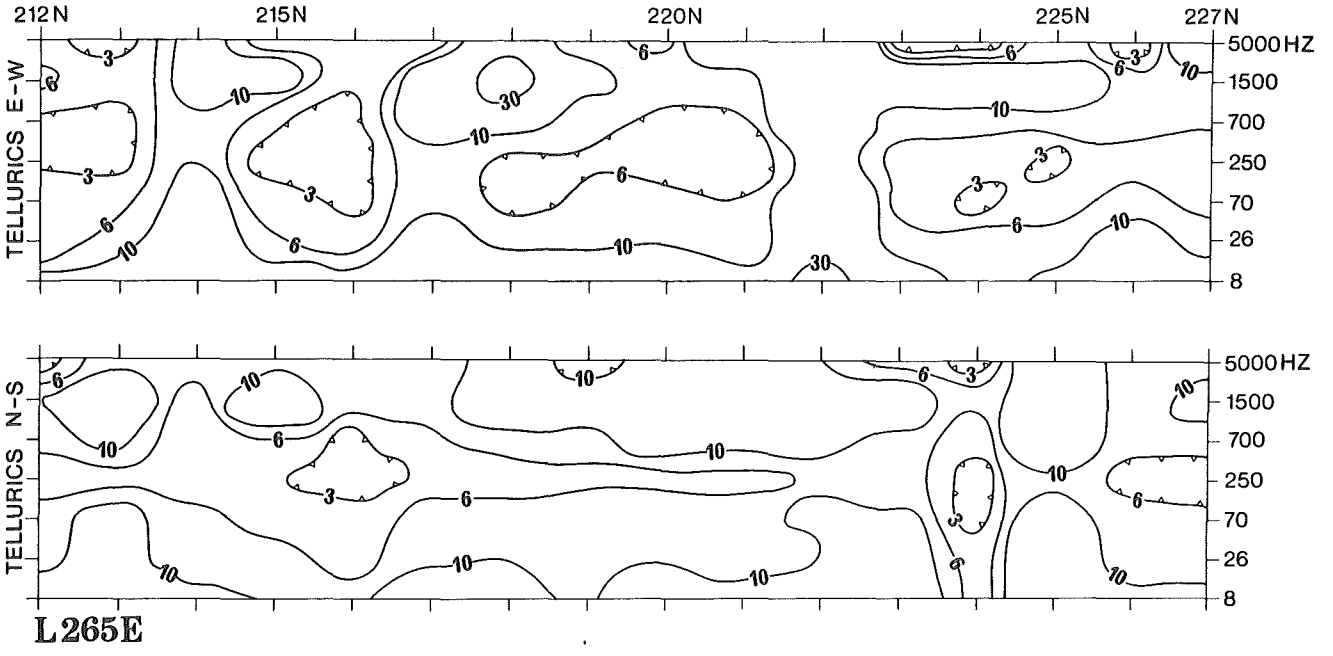

FIGURE 11: Same as Figure 10 for Line 265E

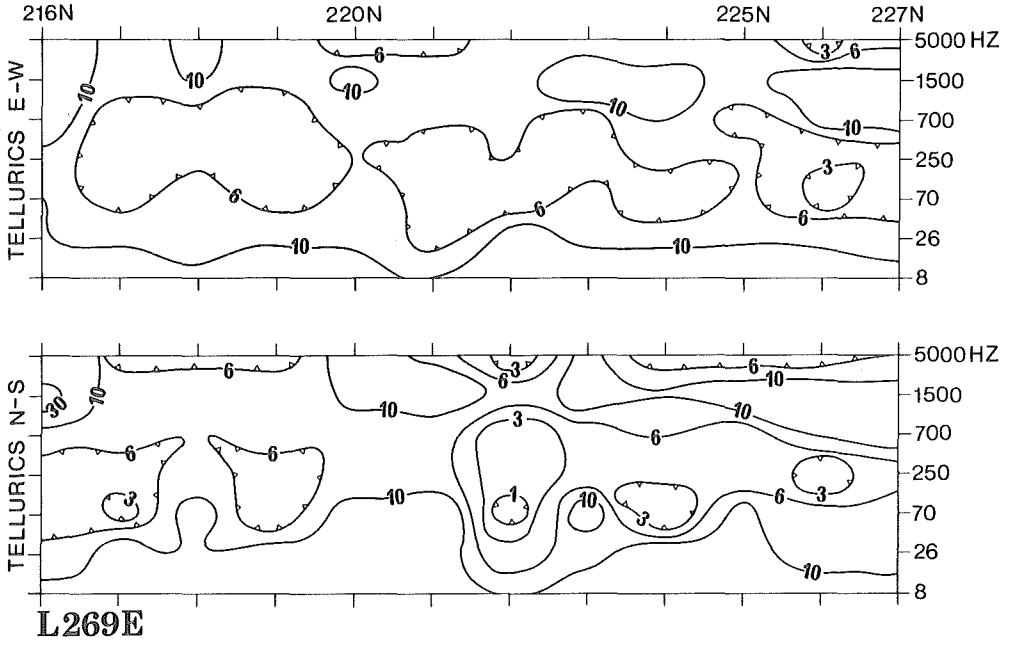

FIGURE 12: Same as Figure 10 for Line 269E

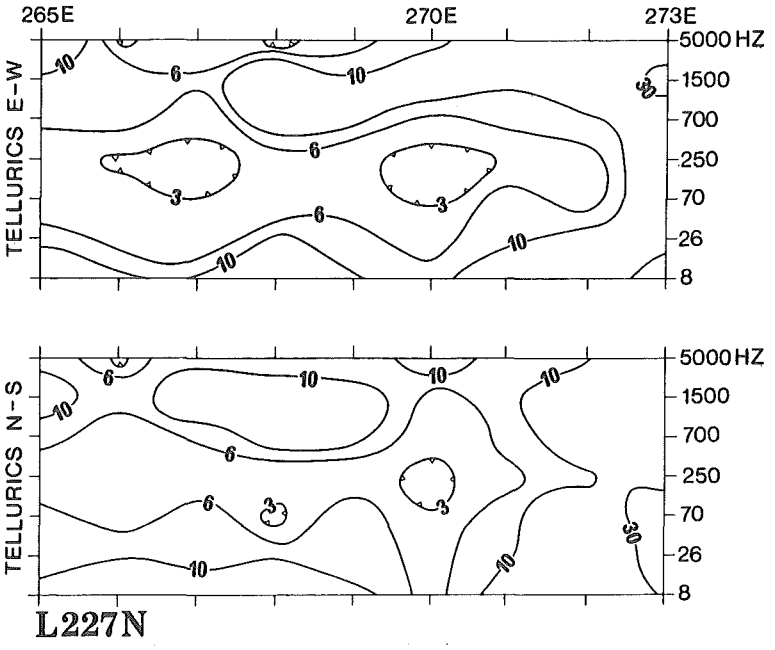

FIGURE 13: Same as Figure 10 for Line 227N

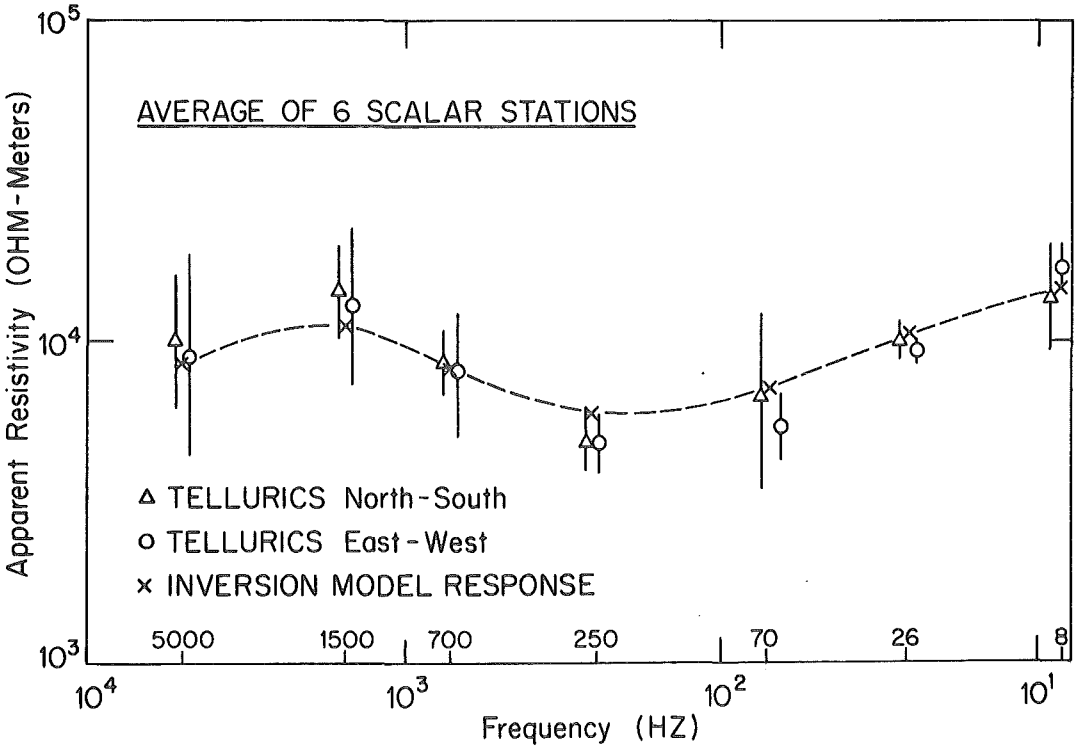

FIGURE 14: Averaged Scalar AMT Data from Six Stations with the Telluric Dipole North-South and East-West [See Table 2 for stations used.]

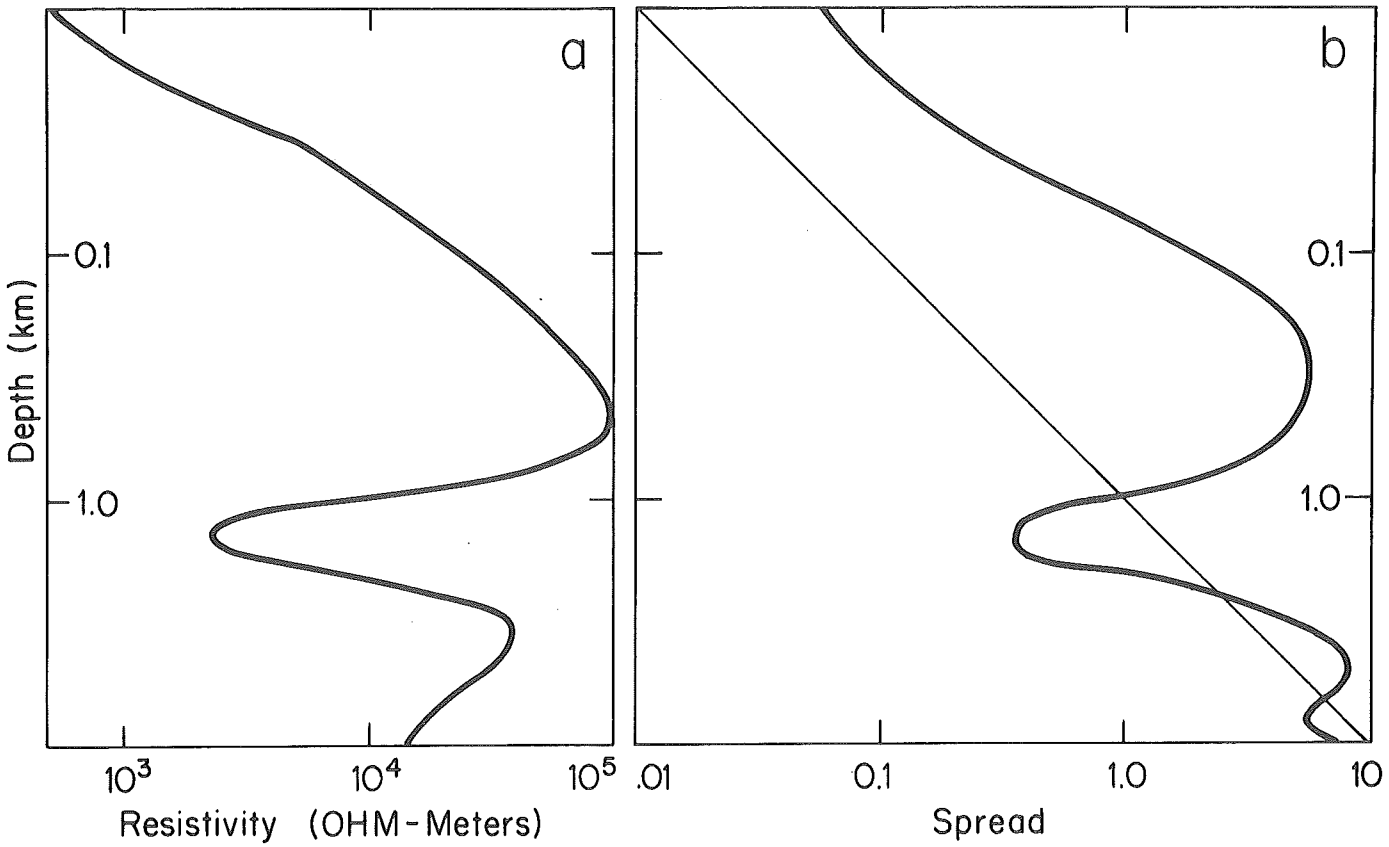

FIGURE 15: Same as Figure 6 for the Averaged Scalar AMT Data Measured in the Telluric North-South Direction